Materials Chemistry and Physics 230 (2019) 239–248

Contents lists available at ScienceDirect

Materials Chemistry and Physics

journal homepage: www.elsevier.com/locate/matchemphys

The building of molecular imprinted sites on the Stöber spheres of resorcinol-formaldehyde resin: In situ organic vs. inorganic imprinting method

Jun Ye[a,b,c,1], Xing Li[a,b,c,1], Qiyan Li[c], Teng Qiu[a,b,c,*], Longhai Guo[c], Lifan He[b,c], Xiaoyu Li[a,b,c,**]

[a] State Key Laboratory of Organic-Inorganic Composites, Beijing University of Chemical Technology, Beijing, 100029, PR China
[b] Key Laboratory of Carbon Fiber and Functional Polymers, Ministry of Education, Beijing University of Chemical Technology, Beijing, 100029, PR China
[c] Beijing Engineering Research Center of Synthesis and Application of Waterborne Polymer, Beijing University of Chemical Technology, Beijing, 100029, PR China

ARTICLE INFO

Keywords:
Microsphere
Resorcinol-formaldehyde resin
Molecular imprinting
Photocatalytic degradation
Bisphenol A

ABSTRACT

Functional microspheres with subtle designed molecular recognition sites is much highlighted in recent days. We here study the in situ molecular imprinting in the Stöber synthesis of resorcinol-formaldehyde (RF) microspheres, and two different approaches are demonstrated. One approach is named as organic molecular imprinting, during which the target molecules of bisphenol A (BPA) are incorporated as the template in the gelation of RF resin. The other is named as inorganic molecular imprinting, during which the template is introduced together with inorganic precursor of titanate. The sizes of the produced spheric particles are found to rely on the ratio of ethanol/water in the reaction medium. Recognition sites which are BPA specific have been detected on both the RF and RF-carbon/TiO_2 spheres, and the latter show slightly higher capacity and selectivity in rebinding tests. Importantly, the integration of the photo active nano TiO_2 on the submicron spheric carbon support with BPA imprinted sites is of unique advantages, which exhibits as the specific high photocatalytic efficiency on BPA degradation under UV light. This, together with the high selectivity, substantial efficiency and operable uniform size of the composite spheres would be useful in the engineering for environmental and analysis fields.

1. Introduction

Functional spheric particles built by both organic polymer and carbon with submicron sizes have attracted great interests recently due to their wide applications in the fields [1,2]. Being a kind of popular resin as well as good carbon source, a great deal of labor has been devoted in the synthesis of resorcinol-formaldehyde (RF) resin based microspheres [3,4]. One of the most highlighted approaches is the Stöber method through the organic sol-gel reaction of resorcinol and formaldehyde, in which it is possible to achieve excellent control on spheric shapes and sizes of the particle products [5,6]. In addition, the high activities of the abundant aromatic rings and hydroxyl groups in RF network provide opportunities for the building of subtle structures in/on the microspheres for functional applications [7,8]. Moreover, the especially high efficiency for carbon formation of RF provides the RF-based microspheres a window towards a spectrum of highlighted applications as the modern carboneous material in heterogeneous catalysis, drug delivery and energy-conversion/storage, etc [9]. However, it should be remarked that all the advanced applications of RF and RF-carbon (RF-C) are relying on the further fabrication of functional fine structures superposed on the microspheric matrix, which is a just developed topic and open for the different designs and various applications.

The building of artificial molecular recognition system is another hot topic in material science [10,11]. One typical achievement in the field is the molecular imprinted particles (MIP) [12,13]. Different polymerization reactions involving the various organic monomers or inorganic precursors have been applied in the synthesis of MIP [14,15]. The products have been found of capability to recognize and selectively bind with the target molecules in complicated matrix, especially remarkable when be applied in the detection or separation of the environmental contaminates with low concentration but high expose

* Corresponding author. State Key Laboratory of Organic-Inorganic Composites, Beijing University of Chemical Technology, Beijing, 100029, PR China.
** Corresponding author. Key Laboratory of Carbon Fiber and Functional Polymers, Ministry of Education, Beijing University of Chemical Technology, Beijing, 100029, PR China.
E-mail addresses: qiuteng@mail.buct.edu.cn (T. Qiu), lixy@mail.buct.edu.cn (X. Li).
[1] Contribute equally to the work.

https://doi.org/10.1016/j.matchemphys.2019.03.057
Received 7 June 2018; Received in revised form 21 January 2019; Accepted 18 March 2019
Available online 26 March 2019
0254-0584/

risks. One typical example of such contaminates is bisphenol A (BPA), one endocrine disrupting chemical but is popular used in polymer resin products and has been a serious threaten for the safety of water matrix.

The principle of molecular imprinting is the temporary incorporation of the template molecules within the polymer network during its crosslinking so that the molecular information of the target can be immobilized. Accordingly, we wonder if the imprinting process could be superposed on the organic sol-gel reaction of RF resin to introduce BPA recognition sites on the microspheric particles [16]. Such in situ imprinting during the synthesis should be much facile because of its simplicity, including that RF-based MIP prepared through this method would be pronounceable taking the advantages of both the controllable morphology and molecular recognition capability [17].

The direct imprinting of BPA on RF network is possible considering their structural similarities. Hydrogen-bonding (H-bonding) and π-π interactions can be utilized for their complexion. The reversible non-covalent incorporation is of benefits for the following template removal [18,19]. Besides, the active phenolic hydroxylic groups can also be utilized for the surface modification on RF particles [20,21], which means a surface MIP [22]. The popular method for template removal is solvent extraction. Alternatively, high-temperature calcination has also be reported as another choice in the building of molecular imprinted inorganic frame work, with the advantage of that the gel mineralization and the template removal can be efficiently combined in the same process [23,24]. We here are also interested in the calcination method considering the capability of RF to transform into carbon.

Herein, we develop two different approaches for the in situ BPA imprinting in the Stöber synthesis of RF resin. One approach is direct imprinting, during which the template is added directly in the condensation of resorcinol and formaldehyde, and removed through solvent extraction. The other approach is inorganic imprinting, during which the template is added in the same reaction pot but after the polymerization of the organic resin together with the batch of inorganic precursor of tetrabutyl orthotitanate. The following hydrolysis and condensation of titanate is anchored on RF surfaces by electrostatic interaction [25,26], while the template is incorporated in situ in the titanate network through hydrogen bonding [21,27]. The template in the inorganic imprinting is removed by calcination. At the same time, RF particles with their surface titanate layers can transform into RF based carbon (RF-C) coated by nano-anatase TiO_2 [28]. The successful building of BPA recognition sites on both kinds of the imprinted products have been verified by a series of static and competitive rebinding tests. Furthermore, RF-C/TiO_2-MIP got through the inorganic imprinting approach is unique for its additional activity as BPA specific photocatalyst, whose performance is also involved in the following work.

2. Experimental

2.1. Materials and apparatus

BPA was from Country Medicine Reagent Co. Ltd., Shanghai, China. Resorcinol, hydroquinone (HQ), phenol and polyvinyl alcohol (PVA1788) and formaldehyde solution (37 wt%, aq) was from Tianjin Guangfu Fine Chemical Institute, Tianjin, China. Tetrabutyl orthotitanate ($Ti(OBu)_4$) was from Shanghai Kefeng Chemistry Co., Ltd., Shanghai, China. Ammonia and ethanol was provided by Beijing Chemical Works, Beijing, China. All the reagents were of analytical grade and used as received. Water used in the work was self-made deionized (DI) water.

The scanning electron microscopy (SEM) used in the work was Hitachi S-570, Japan. Energy dispersive spectrometer (EDS) was provided using an energy dispersive spectrometer integrated on SEM. Transmission electron microscopy (TEM) was taken by Tecnai G2 F30 (FEI). X-ray diffraction (XRD, D8 Focus, Bruker) measurements were carried out using Cu Kα radiation at a tube current of 40 mA and a voltage of 40 kV. Infrared spectra were determined by Bruker Tensor 37 Fourier transform infrared (FTIR) spectrometer. Ultraviolet (UV) spectrophotometer (UV-3150, Shimadzu, Japan) was applied to monitor the concentration of BPA in solutions. The surface area analysis was

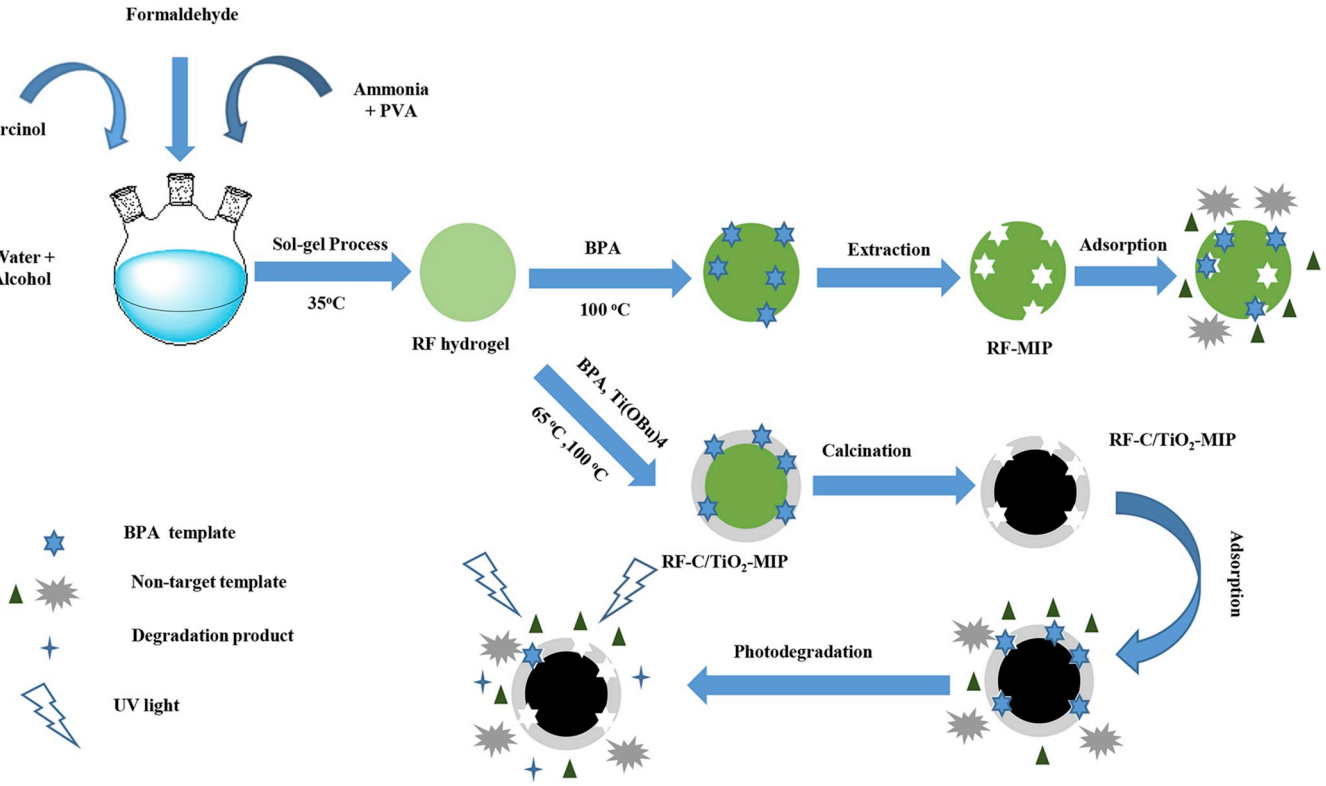

Scheme 1. The synthesis, rebinding and photo degradation process of RF-MIP and RF-C/TiO_2-MIP.

performed using Brunauer-Emmett-Teller (BET) nitrogen adsorption method on ASAP 2046, Micromeritics. Before the measurements, the samples were outgassed for at least 24 h at 100 °C.

2.1.1. Synthesis of RF-MIP (organic imprinting approach)

As shown in Scheme 1, in a typical synthesis, resorcinol (2.0 g) was added in a flask containing PVA (0.6 g), ethanol (100 mL) and water (180 mL). After stirring 20 min at room temperature, $NH_3{\cdot}H_2O$ (1.0 mL, 22–25 wt%) was added into the flask, followed by the dropwise injection of formaldehyde solution (2.8 mL). The stirring speed was constant at 350 rpm, and the temperature was set at 35 °C for 24 h. BPA (0.8 g) was added into the flask for the complex with the phenolic prepolymer. Then the temperature was elevated to 100 °C for another 24 h for RF gelation. The system was cooled down to room temperature to stop the reaction. The solid product was isolated by centrifugation. The template was extracted out through Soxhlet using a mixed solvent of anhydrous methanol and acetic acid with a volume ratio of 9:1 for 24 h. The product was dried in a vacuum oven at 110 °C for 36 h. The red-brown powder was obtained as RF-MIP. The none-imprinted sample is also synthesized via the same procedure but without the addition of the template. The corresponding product is named as RF-NIP.

2.1.2. Synthesis of RF-C/TiO_2-MIP (inorganic imprinting approach)

The polymerization of RF was similar as described above. The only difference is on the addition of BPA. After the 24 h of reaction at 35 °C and another 24 h reaction at 100 °C, the dispersion was subsequently cooled to 65 °C for the addition of the ethanol solution of tetrabutyl titanate (6 g in 80 mL of ethanol) at the rate of 3.0 mL min^{-1}. At the same time, the ethanol solution of BPA (0.8 g in 40 mL ethanol) was injected dropwise through a separated funnel. After the addition, the temperature rose to 100 °C which was kept for 14 h. After the dispersion was cooled to room temperature, the solid product was isolated by centrifugation and washed by DI water for at least 5 times. The wet gel was dried at 100 °C for 24 h in a vacuum oven, calcined under N_2 atmosphere at 350 °C for 2 h and then at 550 °C for another 4 h in a tube furnace. The heating rate was 1 °C·min^{-1}. The final product is named as RF-C/TiO_2-MIP. The none-imprinted sample was also synthesized via the same procedure but without the addition of the template. The corresponding product is named as RF-C/TiO_2-NIP.

2.2. Rebinding capacity and selectivity

The capacity, isotherm and kinetics of BPA rebinding on the products was tested by batch static adsorption. Typically, 0.15 g of the tested sample was dispersed in a conical flask and mixed with 150 mL of the aqueous solution of BPA in 100 mg L^{-1} (initial concentration). The mixture was oscillated at 25 °C using a magnetic stirring in the absence of light. Samples were taken out at different time intervals and purified via centrifugation at 12000 rpm for 10 min and then filtration by 0.22 μm microfiltration membrane. The concentration of BPA in the solution was analyzed by UV-vis spectroscopy tested at a wavelength of 277 nm. The reported results were obtained on the average of the data on no less than three repeated experiments. The rebinding capacity (Q) was calculated as follows [31]:

$$Q = \frac{(C_0 - C_t)V}{W} \tag{1}$$

where C_0 (mg·L^{-1}) is the initial concentration of BPA, C_t (mg·L^{-1}) is the BPA concentration at different time, V (mL) is the volume of BPA solution, and W (g) is the mass of the tested samples. Pseudo-first-order and pseudo-second-order kinetics models were used to fit the rebinding kinetics, respectively. The equations are expressed as follows [31]:

$$\mathrm{In}(Q_e - Q_t) = \mathrm{In}Q_e - k_1 t \tag{2}$$

$$\frac{t}{Q_t} = \frac{1}{k_2 \times Q_e^2} + \frac{1}{Q_e} \times t \tag{3}$$

where Q_e (mg·g^{-1}) is the rebinding capacity at equilibrium, Q_t (mg·g^{-1}) is the rebinding capacity as the function of the time of t (min), k_1 (min^{-1}) and k_2 (g·mg^{-1}·min^{-1}) is the constant of pseudo-first and second order kinetics, respectively.

To test of the rebinding isotherm, 0.01 g of sphere sample was separately mixed with 10 mL of BPA solutions with specific initial concentration ranging from 25 to 600 mg L^{-1}. The mixtures were oscillated for 24 h at 25 °C in the dark. Scatchard equation was employed to evaluate the maximum rebinding capacity, expressed as the following equation [32]:

$$\frac{Q}{C} = \frac{Q_{max}}{K_d} - \frac{Q}{K_d} \tag{4}$$

where C (mg·L^{-1}) is the equilibrium concentration of BPA in liquid, Q_{max} (mg·g^{-1}) is the maximum rebinding capacity of BPA and K_d (mg·L^{-1}) is the equilibrium dissociation constant of the rebinding sites.

To evaluate the rebinding selectivity, 20 mL solution of BPA, phenol and HQ were used with individual initial concentration fixed in 100 mg L^{-1}. In the competitive tests, the binary solutions of BPA and phenol or HQ were used, and each of them is of the individual initial concentration of 100 mg L^{-1}. The detection wavelength for UV-vis was 277 nm for BPA, 270 nm for phenol and 289 nm for HQ, respectively. The rebinding capacity of BPA, phenol and HQ is denoted as Q_{BPA}, Q_{phenol} and Q_{HQ}, respectively, which is calculated according to equ. (1).

2.3. Photocatalytic activity and selectivity

Photocatalytic activity was evaluated by monitoring the BPA concentration in aqueous solution under UV irradiation. 0.1 g of the photocatalyst was dispersed into 400 mL of BPA solution whose initial concentration was 25 mg L^{-1}. After stirring in dark for 2 h, the dispersion was exposed to the irradiation supplied by a UV lamp (17 W, 254 nm) with 10 cm distance away from the solution surface. The concentration of BPA was measured and plotted as the function of time. To evaluate the photocatalytic selectivity, 400 mL of binary solution of BPA and phenol with individual initial concentration of 25 mg L^{-1} was used. The reported results were obtained on the average of the data on no less than three repeated experiments. The photocatalytic degradation of BPA was analyzed by pseudo-first-order kinetics as follows [33]:

$$\mathrm{In}\left(\frac{C_0}{C_t}\right) = kt \tag{5}$$

where C_0 (mg·L^{-1}) is the initial concentration of BPA, C_t (mg·L^{-1}) is the concentration of BPA at different UV exposure time of t (h), and k (h^{-1}) is the reaction rate constant.

3. Results and discussion

3.1. Synthesis of RF and RF-C/TiO_2 MIP

The two different approaches for the in situ BPA imprinting are all based on the organic Stöber synthesis of RF resin thorough the polycondensation/crosslinking mechanism: formaldehyde first reacts with resorcinol to form hydroxymethyl ($-CH_2OH$) derivatives of the three chemicals, which subsequently form methylene ($-CH_2-$) and methylene ether ($-CHOCH_2-$) bridged gel networks through condensation. The difference is on the temperature: in the synthesis of RF-MIP, there should be more hydroxyl and ether groups, most of which would be decomposed during the calcination for RF-C/TiO_2-MIP as the leaving of the methylene happened at the temperature range between 300 and 500 °C. The TEM of synthesized RF and RF-C/TiO_2 MIP and the influence of water/ethanol are shown in Fig. 1.

It is clearly shown in the TEM images that the water/ethanol

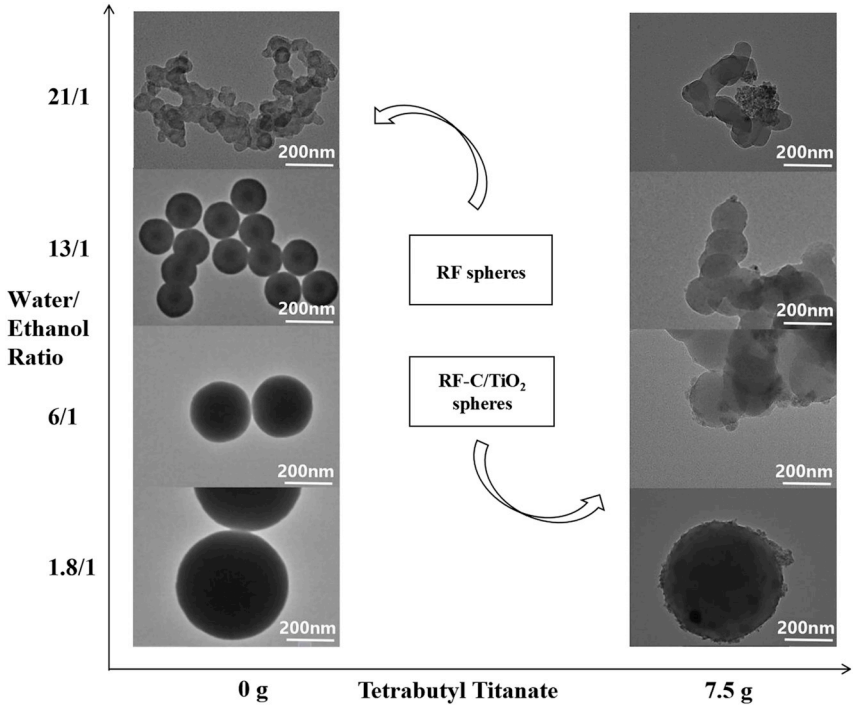

Fig. 1. TEM images of RF and RF-C/TiO_2-MIP under different water/ethanol ratio.

volume ratios have strong influence on the size of RF-MIP. The phenomena suggests an heterogeneous system controlled by interfacial tension [29,30]. Under the water/ethanol ratio of 1.8/1 (v/v), regular global spheres are observed with the average diameter of 500 nm. By increasing the water/ethanol ratio, the sphere size decreases from 500 to 170 nm. But, the spherical morphology is well sustained until the water/ethanol ratio rises to 21/1. The high content of water is facilitated for small particle production, and these small particles below 50 nm are with strong trend to agglomeration.

The size of RF-C/TiO_2-MIP is depended on its RF-template. However, the introduction of titanate into the RF hydrogel tends to trigger the particle agglomeration to happen under relatively lower water/ethanol ratio including 13/1 and 6/1. After the exclusion the cases where the irregular products are formed, we find the optimal condition for uniform products, which can only be achieved under lowest water/ethanol ratio of 1.8/1. The TiO_2 decoration on RF-C particles under this condition is indicated by the coarse edges and dark dots on the large spheres as compared with RF particles [5,34].

The irregular packing of nano-TiO_2 on the surface of RF-C is clearly displayed in the TEM image in Fig. 2a. In Fig. 2b, the nano-sized grain of TiO_2 can be distinguished, whose lattice fringes are of the distance of 0.36 nm. The typical SEM images of RF and RF-C/TiO_2 are shown in Fig. 3. The obvious difference of the coarse surfaces of RF-C/TiO_2 from the smooth surfaces of RF spheres provides another evidence for the incorporation of nano-TiO_2 onto RF-C. EDS result of RF-C/TiO_2-MIP has been shown as Fig. 3c. The emergence of the characteristic peak of Ti verifies again the loading of TiO_2. The crystal structure of nano-TiO_2 on RF-C composite is identified by XRD. As shown in Fig. 4, the characteristic peaks at 2θ of 25.24°, 37.94°, 48.03°, 53.96°, 54.92° and 62.56° are corresponding to (1 0 1), (0 0 4), (2 0 0), (1 0 5), (2 1 1) and (2 0 4) reflections of anatase, respectively. Since there is no sign of the characteristic peak of 27.4° (rutile) or 30.8°(brookite), it is reasonable for us to believe that anatase should be dominated in our TiO_2. Scherrer equation [35] is applied to calculate the average size of nano grains, which is 6.62 nm. It has been suggested that incorporation of nano anatase with carbon support should be in favor of the enhancement of photocatalytic activity [17].

Nitrogen adsorption-desorption isotherms of our two kinds of MIP

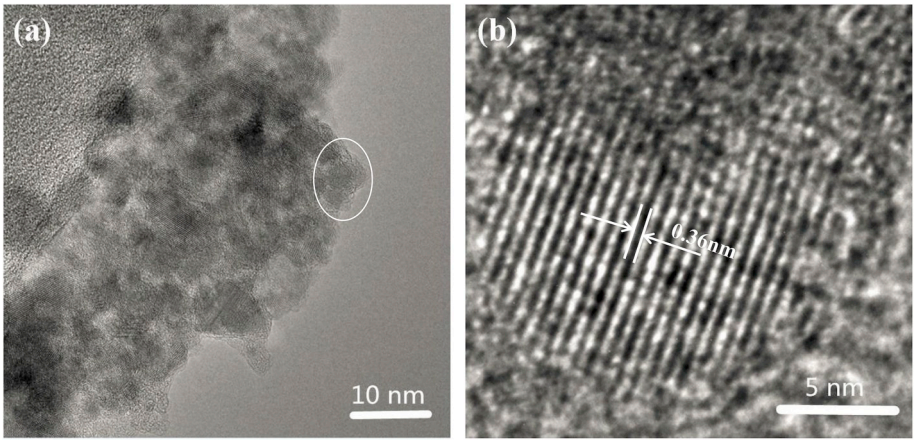

Fig. 2. (a)Zoom-in TEM images of RF-C/TiO_2-MIP and (b) High resolution image of TiO_2 on RF-C/TiO_2-MIP.

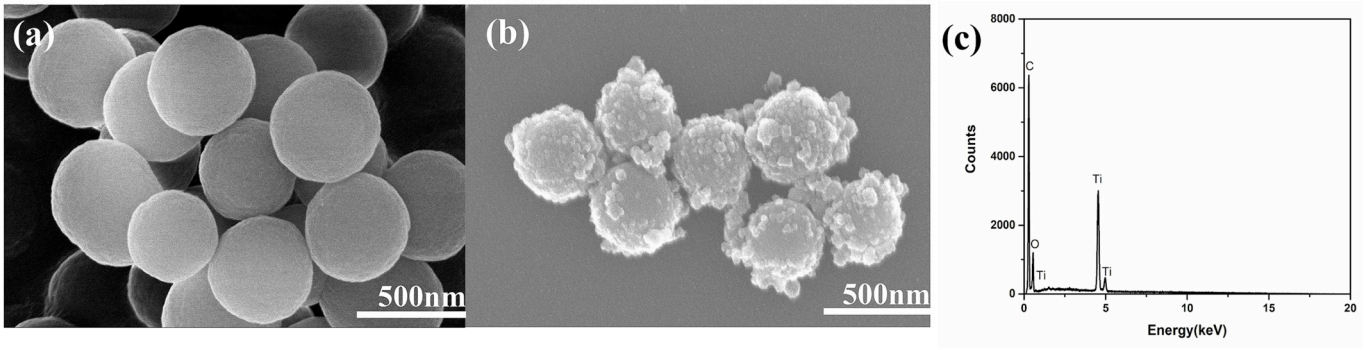

Fig. 3. (a) SEM image of RF-MIP; (b) SEM image of RF-C/TiO_2-MIP; (c) EDS of RF-C/TiO_2-MIP.

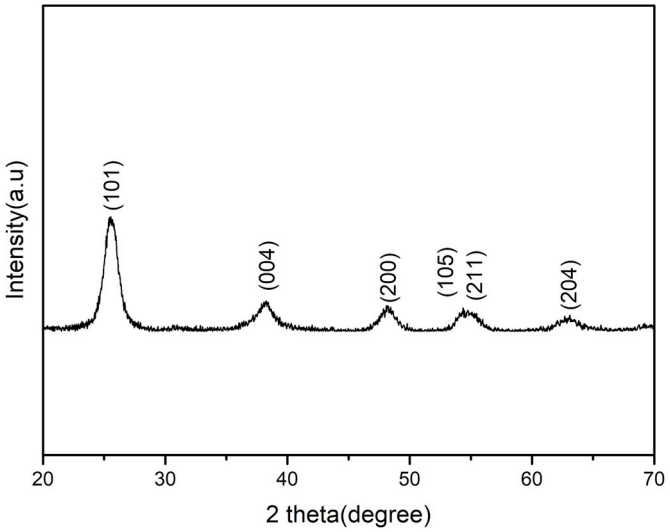

Fig. 4. XRD patterns of RF-C/TiO_2-MIP.

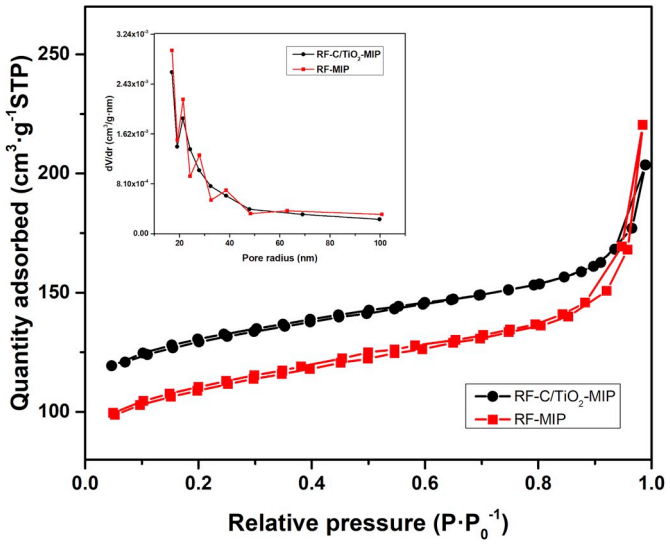

Fig. 5. Nitrogen adsorption-desorption isotherms of RF-C/TiO_2-MIP and RF-MIP.

samples are displayed in Fig. 5. We can see the typical "type IV" profiles in the figure. The BET surface areas are also calculated, which is 416 $m^2 g^{-1}$ for RF-MIP with a total pore volume of 0.35 $cm^3 g^{-1}$. The pore size distribution shown as the insert presents a peak at 21.4 nm. For RF-C/TiO_2-MIP, the BET surface area is 358 $m^2 g^{-1}$, and the total pore volume is calculated to be 0.31 $cm^3 g^{-1}$. The pore size distribution is also found in the insert figure. The profile is similar with that of RF-MIP, but consists of three sharp peaks corresponding to the size of 21.4 nm, 27.9 nm and 38.6 nm, respectively. The loading of TiO_2 reduces the specific surface area and broadens the pore size distribution, which may be explained by the embedding of some of the TiO_2 into the carbon matrix. However, the BET surface area maintains still at the same level. The formation of mesopores is of advantage for the diffusion of small molecules; the relatively large specific surface area provides efficient contacting sites. Both of the features are positive for the target molecules to rebind on polymer particles.

The incorporation and removal of BPA for imprinting can be illustrated by FTIR. As shown in Fig. 6a, the band at 832 cm^{-1} characteristic in the spectrum of BPA appears in RF spectrum before the extraction treatment, indicating the incorporation of BPA. The band disappears in RF-MIP, indicating the removal of BPA. In addition, identical groups for RF resin have also been seen: the band at 3023 cm^{-1} is attributed to the C-H groups on the benzene rings, and the band at 3386 cm^{-1} is attributed to the -OH groups.

Similar results can also be achieved in the case of inorganic imprinting. Although the band 832 cm^{-1} is not as identical as in the pure organic samples in Fig. 6b, the incorporation of BPA on RF/TiO_2 before calcination can be assured by the three BPA bands at 1360 cm^{-1}, 925 cm^{-1} and 832 cm^{-1}. All the three peaks are disappeared in the spectrum of RF-C/TiO_2-MIP after calcination. The emerging and disappearing of BPA peaks clearly fits the designed imprinting process of BPA on RF-C/TiO_2-MIP. In addition, the band at 590 cm^{-1} is related to the stretching vibration of Ti-O-Ti. The peak at around 1225 cm^{-1} is corresponding to C-O-Ti bond, indicating the complex of TiO_2 with carbon framework. Although most of the organic groups on RF have been reduced or eliminated in RF-C/TiO_2-MIP, part of phenol groups and aromatic rings are survival, suggesting by the bands at 3392 cm^{-1} and 1612 cm^{-1}. The hydroxyl and aromatic groups as well as the cavities caused by the leaving of template molecules can all serve for the recognition of the target BPA in their rebinding experiments [7,16].

3.2. Recognition in rebinding

We here apply the pseudo-first-order and pseudo-second-order models to evaluate the rebinding kinetics of BPA on MIP samples, respectively. As shown in Fig. 7, the rebinding kinetics for BPA on RF-MIP and RF-C/TiO_2-MIP fitted by the pseudo-first-order model (Fig. 7a) is not as well as by the pseudo-second-order model (Fig. 7b), which is also suggested by the different correlation coefficients (R^2) in Table 1. Accordingly, the rebinding of BPA on our RF based MIP is affected by the chemisorption mechanism. The sharp increase on equilibrium capacity and rebinding rates are observed on the two MIP samples in comparison with the NIP ones. The kinetics of RF-NIP and RF-C/TiO_2-NIP are also plotted in the figure with the fitting parameters included in Table 1, which reveals a relatively slower absorption process. The values of k_2 are similar of the two MIP samples, suggesting the acceleration on

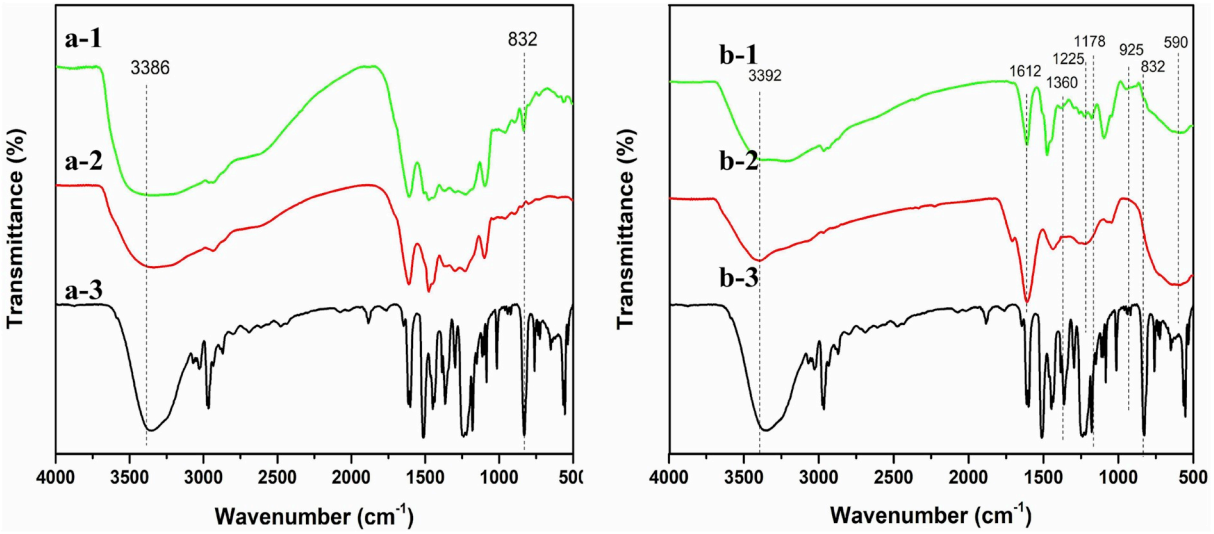

Fig. 6. FTIR spectra of (a-1) RF-before the extraction, (a-2) RF-MIP, (a-3) BPA; (b-1) RF/TiO_2 before calcination, (b-2) RF-C/TiO_2-MIP and (b-3) BPA.

rebinding rates should be attributed to the building of BPA imprinted sites on the microspheres.

The rebinding isotherms of BPA on RF-MIP and RF-NIP are shown in Fig. 8a–1. The rebinding capacities increase with the increase of BPA concentration. The difference is on the slopes:the growth rate of RF-MIP is much higher than that of RF-NIP, indicating the rapid rebinding of the target molecules on the specifically imprinted cavities.

Scatchard equation is then applied to evaluate the heterogeneity of the different sites on MIP [36]. The two lines on the Scatchard profile of RF-MIP in the main figure in Fig. 8a–2 represent two types of rebinding sites, i.e. nonspecific and specific sites. K_d and Q_{max} for the specific rebinding sites on RF-MIP is calculated to be 0.26 mg L^{-1} and 58.66 mg g^{-1}, respectively. K_d and Q_{max} for the nonspecific rebinding sites on RF-MIP microspheres is 2.50 mg L^{-1} and 377.62 mg g^{-1}, respectively. In contrast, the Scatchard profile of RF-NIP is fitted well by a single line, suggesting only one kind of rebinding sites which is non-specific [37].

The figures in Fig. 8b–1 display the rebinding isotherm of BPA on RF-C/TiO_2. Similar up-going trends of rebinding capacities are found as the function of the BPA concentration, with the slope of MIP profile larger than that of NIP. The existing of specific as well as the non-specific sites on RF-C/TiO_2-MIP can also be evaluated by the Scatchard plot. As shown in Fig. 8b–2, the rebinding profile of RF-C/TiO_2-MIP is also divided into two straight lines. The value of K_d and Q_{max} is 0.17 mg L^{-1} and 54.03 mg g^{-1} for the upper line (specific), and 0.77 mg L^{-1} and 174.55 mg g^{-1} for the under line (non-specific), respectively. Still, there is only one class of rebinding sites on RF-C/TiO_2-NIP, which shows one straight Scatchard line as the insert of Fig. 8b–2.

The formation of specific sites on the two kinds of MIP is further proved by the selectively recognition on BPA from its structural analogs of phenol and HQ. The chemical structures are displayed in Fig. 9a. As shown in Fig. 9b and c, the rebinding of BPA shows obvious distinction with that of phenol and HQ. When RF-MIP is applied whose Q_{phenol} and Q_{HQ} shows no difference in compared with the RF-NIP samples, Q_{BPA} is obviously the highest. As what we have expected, RF-C/TiO_2-MIP also shows obvious rebinding preference for only BPA. It is interesting that Q_{BPA} of RF-C/TiO_2-MIP, which is 19.9 mg g^{-1}, is larger than the value of 15.8 mg g^{-1} of RF-MIP. At first, we tried to explain the difference by different specific areas because of the TiO_2 coating. However, BET characterization gives us the opposite results. So we suppose that the

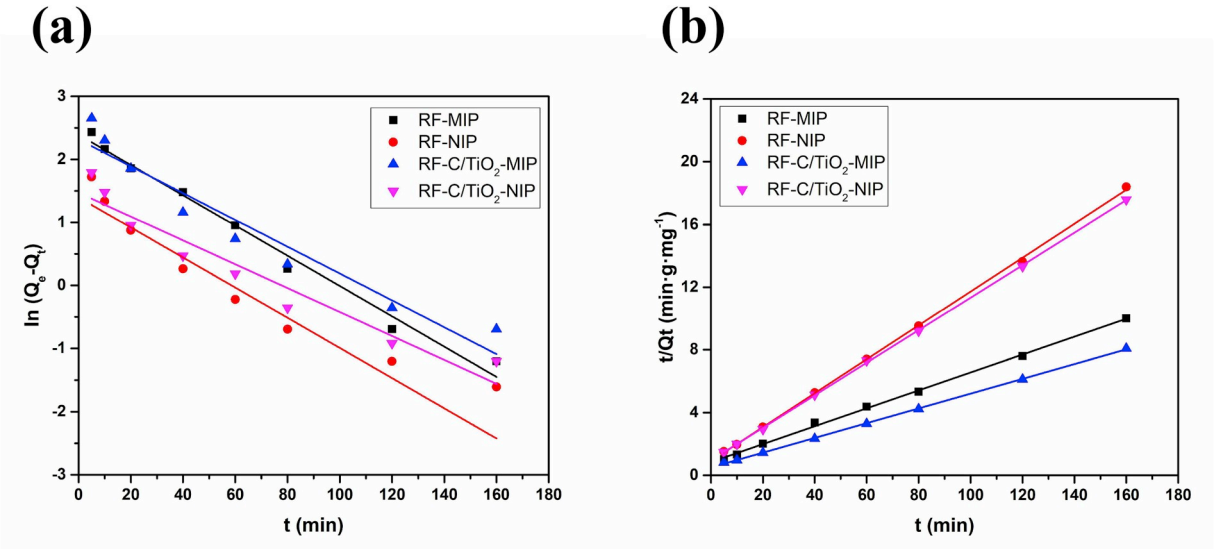

Fig. 7. Rebinding kinetics of (a) RF-MIP, RF-NIP, RF-C/TiO_2-MIP and RF-C/TiO_2-NIP, fitted by pseudo-first-order model; (b) RF-MIP, RF-NIP, RF-C/TiO_2-MIP and RF-C/TiO_2-NIP, fitted by pseudo-second-order model.

Table 1
Parameters for BPA rebinding kinetics.

Samples	$Q_{e,e}$ (mg·g^{-1})	Pseudo-first-order			Pseudo-second-order		
		$Q_{e,c}$ (mg·g^{-1})	k_1 (min^{-1})	R^2	$Q_{e,c}$ (mg·g^{-1})	k_2 (g·mg^{-1}·min^{-1})	R^2
RF-MIP	21.6	10.9	0.024	0.983	17.5	0.004	0.998
RF-NIP	8.90	4.05	0.023	0.859	9.24	0.013	0.999
RF-C/TiO_2-MIP	20.3	10.7	0.022	0.958	21.3	0.004	0.999
RF-C/TiO_2-NIP	9.40	3.69	0.017	0.921	9.63	0.011	0.998

$Q_{e,e}$ is the experimental value of Q_e.
$Q_{e,c}$ is the calculated value of Q_e.

distribution of the MIP sites should be the most responsible. In comparison with the organic imprinting where there are more possibilities for the imprinting sites to be embedded inside the RF spheres, the imprinted sites built by the inorganic imprinting might be of more opportunities to locate on the surface layer. Whatever, the obvious rebinding preference clearly convinces the specialized affinity of RF-MIP and RF-C/TiO_2-MIP to BPA.

The preference of our two kinds of MIP for BPA can be further illustrate by the competitive rebinding experiments. As illustrated in Fig. 10a, Q_{BPA} of RF-MIP in the two binary solutions is similar (15.4 mg g^{-1} and 15.8 mg g^{-1}), are much higher than Q_{phenol} or Q_{HQ}. For RF-C/TiO_2-MIP, as shown in Fig. 10b, Q_{BPA} is also much exceeded over Q_{phenol} and Q_{HQ}. The unique selectivity in competitive adsorption identifies the recognition accuracy of the imprinting sites via two facile in situ methods.

3.3. Photocatalytic activity and selectivity

The additional nano-anatase on RF-C/TiO_2-MIP is well known for its photocatalytic activity. We expect that the composition with target-recognition sites would be of in situ enrichment effect. Moreover, it has also been reported that RF-carbon with sub-micron size is a desirable support for nanoparticles in practical applications [38]. In addition, the non-metal doping of TiO_2 with carbon would cause the narrowing of band gap and the anodic shift of the quasi Fermi potential [39]. Above all suggest the advantage of RF-C/TiO_2-MIP as the catalyst for the photodegradation of BPA. As shown in Fig. 11, the regression curves of natural logarithmic decrements of BPA concentration versus irradiation time are linear, indicating that all the photodegradation follows the pseudo-first-order kinetics. The efficiency of different catalysts on different contaminants can therefore be compared by the slope of the

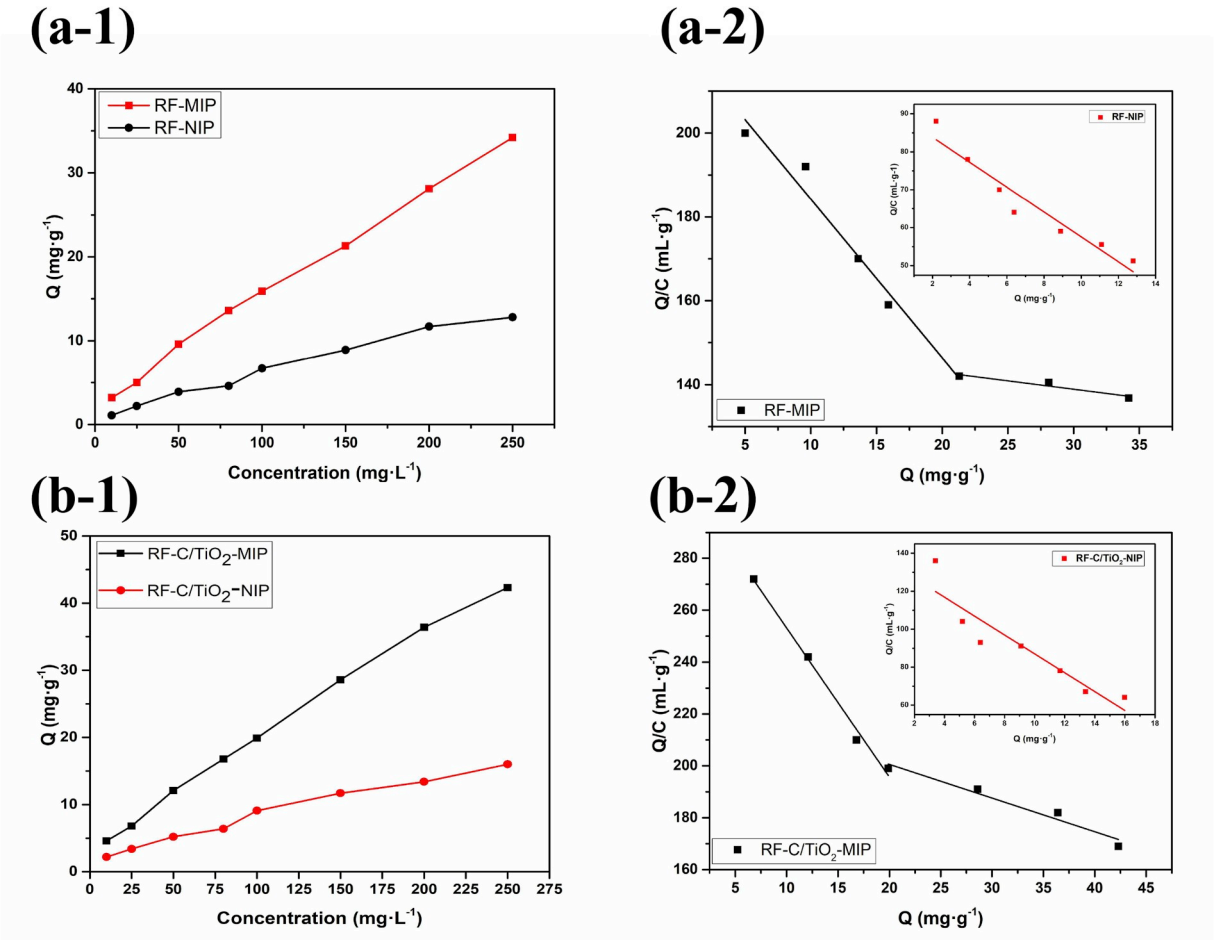

Fig. 8. (a-1) BPA rebinding isotherms for RF-MIP and RF-NIP microspheres; (a-2) Scatchard plot for RF-MIP microspheres (inset: Scatchard plot for RF-NIP microspheres); (b-1) BPA rebinding isotherms for RF-C/TiO_2-MIP and RF-C/TiO_2-NIP; (b-2) Scatchard plot for RF-C/TiO_2-MIP (inset: Scatchard plot for RF-C/TiO_2-NIP).

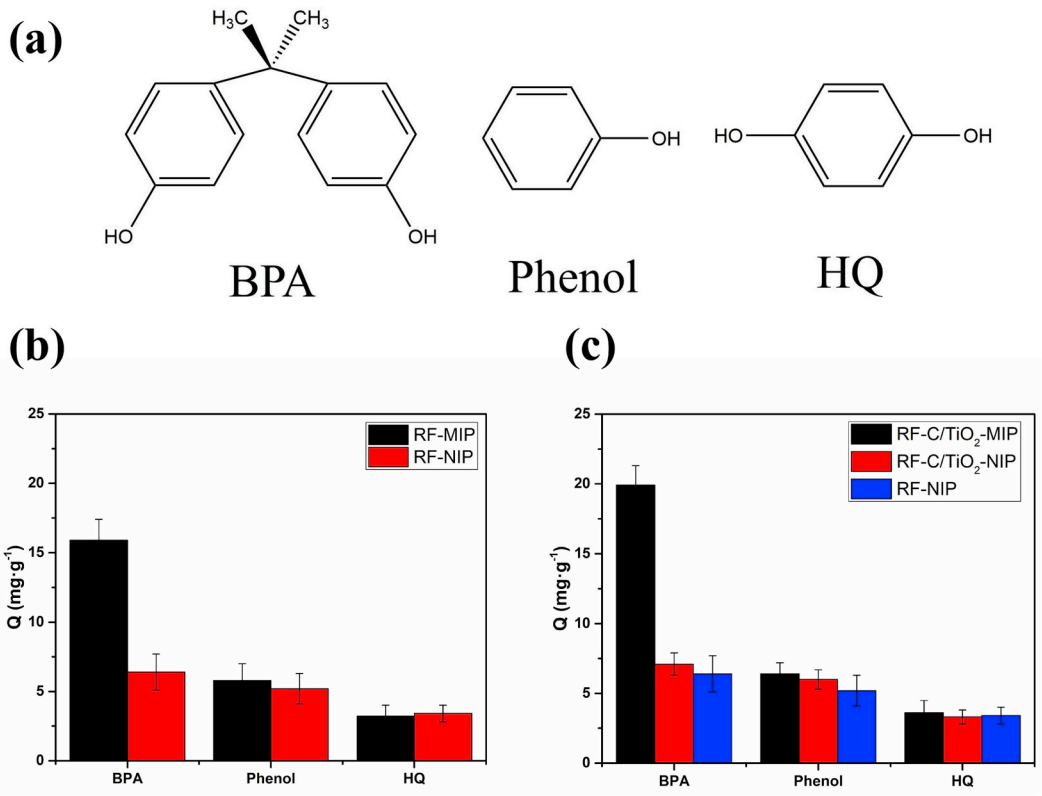

Fig. 9. (a) Structure of BPA, phenol and HQ; (b) Rebinding capacities of BPA, phenol and HQ on RF-MIP and RF-NIP; (c) Rebinding selectivity of BPA, phenol and HQ on RF-C/TiO_2-MIP, RF-C/TiO_2-NIP and RF-NIP.

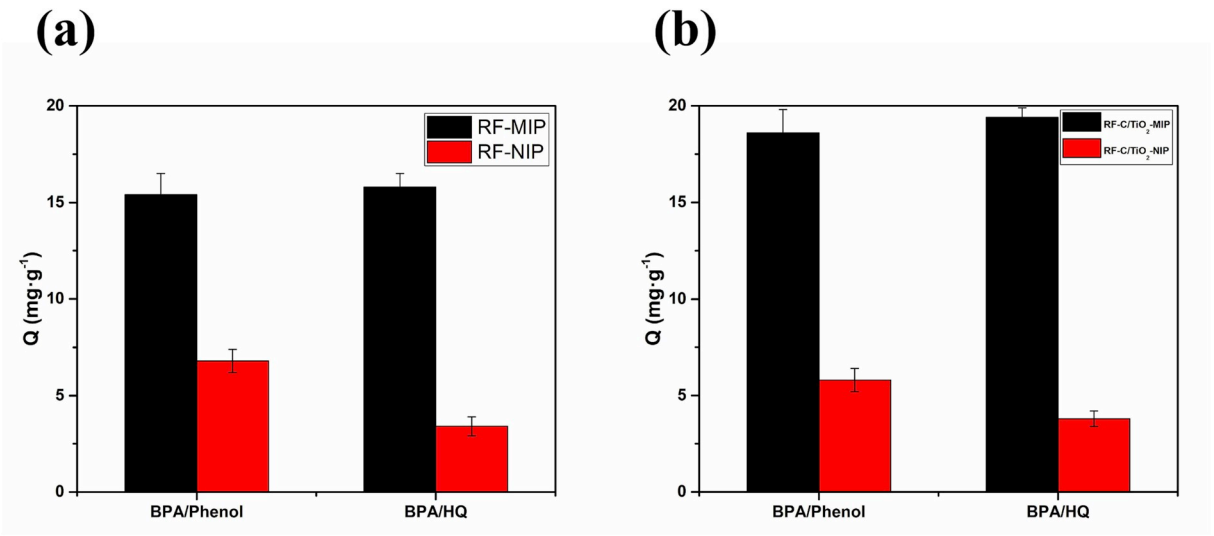

Fig. 10. (a) Competitive rebinding of BPA/phenol and BPA/HQ in binary solutions on RF-MIP and RF-NIP, respectively; (b) Competitive rebinding of BPA/phenol and BPA/HQ in binary solutions on RF-C/TiO_2-MIP and RF-C/TiO_2-MIP, respectively.

kinetic line, which equals to the kinetic constant of *k*.

The effect of different catalysts is shown in Fig. 11a. The slope of the line representing pure TiO_2 is the lowest. TiO_2 here is prepared under the same condition but without the incorporation of RF-resin, whose *k* in the work is 0.0173 h^{-1}. By combining the carbon with nano anatase into RF-C/TiO_2-NIP, we get an obvious higher slope, which is 0.0601 h^{-1}, indicating the positive contribution of the combination of RF-C with photoactive anatase. The steepest line is the one of RF-C/TiO_2-MIP, whose *k* is 0.360 h^{-1}, about five folders of that of RF-C/TiO_2-NIP. Accordingly, it is easy to accept that structure design of RF-C/TiO_2-MIP is of remarkable contribution to enhance the photocatalytic activity.

In order to illustrate selectivity of the catalyst, we carried out photodegradation experiment in the binary solution of BPA and phenol with the results shown in Fig. 11b. Judged by the slopes of the kinetics lines, it is clearly that the degradation of BPA is the fastest, which is in sharp contrast with the slower degradation rate of phenol in the same heterogeneous photocatalytic oxidation degradation system using same RF-C/TiO_2-MIP as the catalyst. On the contrary, the photodegradation of phenol and BPA is of almost no distinguishable low rates under the catalysis of RF-C/TiO_2-NIP, in the same rate level of phenol catalyzed by RF-C/TiO_2-MIP. The above results confirm the high photocatalytic selectivity of RF-C/TiO_2-MIP.

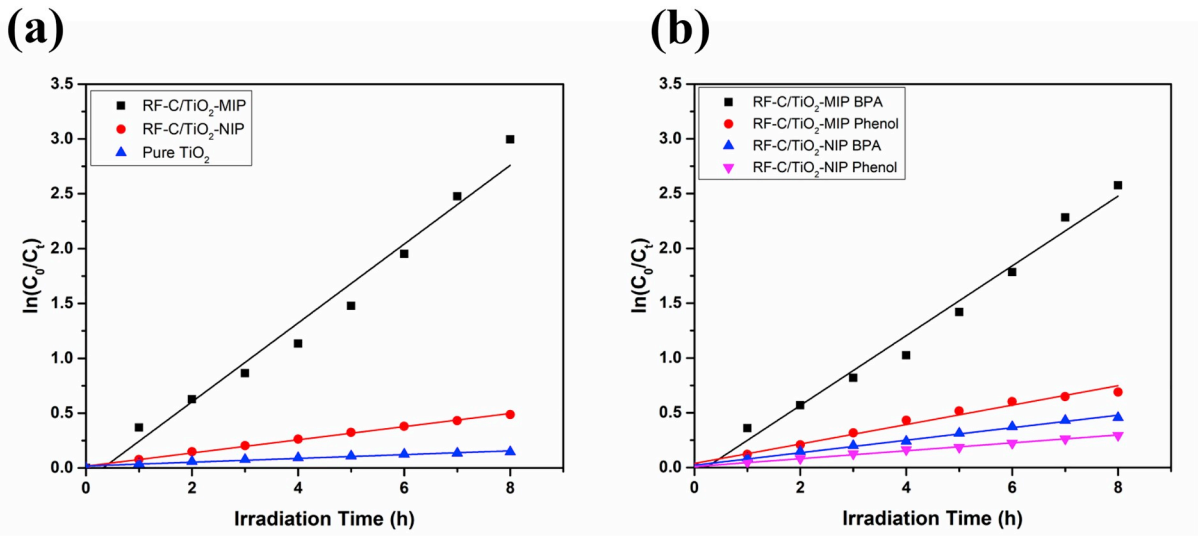

Fig. 11. (a) Photocatalytic degradation of BPA using different photocatalysts; (b) Photodegradation kinetics of BPA and phenol in mixed solutions catalyzed by RF-C/TiO_2-MIP and NIP, respectively.

Table 2
Parameters for BPA rebinding kinetics.

Sample	Type	Synthesis Method	Average Size	t_e (min)	$t_{1/2}$ (min)	Imprinting factor	Degradation rate	Target
1 [40]	MIP	Precipitation polymerization	4 μm	30	6	1.33	74%	BPA
2 [41]	MIP	Pickering emulsion polymerization	70 μm	690	150	1.90	57%	BPA
3 [42]	MIP	Surface imprinted polymerization	300–450 nm	180	20	1.87	60%	BPA
4 [29]	nano-TiO_2	Sol–gel polymerization	10–12 nm	700	400	–	95%	BPA
5 [43]	MIP-TiO_2/GR	Surface imprinted polymerization	250–350 nm	15	4	1.80	12%	BPA
6	RF-MIP	Organic Imprinting	500 nm	60	5	2.10	21%	BPA
7	RF-C/TiO_2-MIP	Inorganic Imprinting	500 nm	60	5	2.52	22%	BPA

Imprinting factor is judged by the equation: $\alpha = Q_{MIP}/Q_{NIP}$.
Degradation rate is judged by the equation: $D = \frac{C_0 - C_e}{C_0} \times 100\%$.

The comparison of our work with others' reports are summarized in Table 2, in which our two products are compared with other MIP as absorbents, and with other TiO_2 based particles as photocatalysts. We can found that in comparison with the absorptive MIP of sample 1 [40], 2 [41] and 3 [42], our spheres are of smallest sizes and consequently fastest adsorption kinetics. Being one kind of photocatalyst, RF-C/TiO_2-MIP is of close efficiency with molecular imprinted TiO_2/graphene composite [43], higher than non-imprinted nano-TiO_2 [29], which is judged by the time parameter of the degradation reaction as $t_{1/2}$. For degradation rate, our particles possess medium level.

4. Conclusions

Two facile in situ methods are developed for the introduction of molecular imprinting template into the Stöber synthesis of RF-based particles. The particles are of well controlled sphere-like morphology and subtle structures as confirmed by a series characterization. Specific sites with BPA recognition ability have been detected on both RF-MIP from organic imprinting and RF-C/TiO_2-MIP from inorganic imprinting, and the latter shows slightly larger capacity and higher selectivity in rebinding tests. Importantly, the carbon spheres decorated by nano TiO_2 are of additional capability to catalyze the photo oxidation degradation. The integration of the nano anatase on carbon microspheres with additional molecular recognition sites shows unique advantages, which exhibits specific high catalysis efficiency on BPA degradation under UV light, which has been supported by the comparison results with related references. Considering the simple synthesis, the high selectivity, substantial efficiency, the well-controlled geometric parameters, the microspheric material can be of potential applications for the perspective of BPA removal from the environment.

Acknowledgments

The authors are grateful for the financial support from the National Key Research and Development Program of China (No. 2016YFC0204402), the National Natural Science Foundation of China (NSFC21304007), and the Fundamental Research Funds for the Central University at Beijing University of Chemical Technology (JD1703 and JD1803).

References

[1] A.M. Elkhatat, S.A. Al-Muhtaseb, Advances in tailoring resorcinol-formaldehyde organic and carbon gels, Adv. Mater. 23 (2011) 2887–2903.
[2] J. Liu, N.P. Wickramaratne, S.Z. Qiao, M. Jaroniec, Molecular-based design and emerging applications of nanoporous carbon spheres, Nat. Mater. 14 (2015) 763–774.
[3] C. Zhang, R. Zhang, X. Gao, C. Cheng, L. Hou, X. Li, W. Chen, Small naked Pt nanoparticles confined in mesoporous shell of hollow carbon spheres for high-performance nonenzymatic sensing of H_2O_2 and glucose, ACS Omega 3 (2018) 96–105.
[4] Y. Wang, B. Chang, D. Guan, X. Dong, Mesoporous activated carbon spheres derived from resorcinol-formaldehyde resin with high performance for supercapacitors, J. Solid State Electrochem. 19 (2015) 1783–1791.
[5] J. Liu, S.Z. Qiao, H. Liu, J. Chen, A. Orpe, D. Zhao, G.Q. Lu, Extension of the Stöber method to the preparation of monodisperse resorcinol-formaldehyde resin polymer and carbon spheres, Angew. Chem. 50 (2011) 5774-5774.
[6] U. Holzwarth, N. Gibson, The Scherrer equation versus the 'Debye-Scherrer equation', Nat. Nanotechnol. 6 (2011) 534.
[7] J. Liu, T. Yang, D.W. Wang, G.Q. Lu, D. Zhao, S.Z. Qiao, A facile soft-template

synthesis of mesoporous polymeric and carbonaceous nanospheres, Nat. Commun. 4 (2013) 2798.
[8] A.H. Lu, G.P. Hao, Q. Sun, Can carbon spheres be created through the Stöber method? Angew. Chem. Int. Ed. 50 (2011) 9023–9025.
[9] S. Mezzavilla, C. Baldizzone, K.J. Mayrhofer, F. Schüth, General method for the synthesis of hollow mesoporous carbon spheres with tunable textural properties, ACS Appl. Mater. Interfaces 7 (2015) 12914–12922.
[10] G.W. Collie, R. Bailly, K. Pulkaziach, C.M. Lombardo, L. Mauran, N. Taibmaamar, J. Dessolin, C.D. Mackereth, G. Guichard, Molecular recognition within the cavity of a foldamer helix bundle: encapsulation of primary alcohols in aqueous conditions, J. Am. Chem. Soc. 139 (2017) 6128–6137.
[11] J.E. Lofgreen, G.A. Ozin, Controlling morphology and porosity to improve performance of molecularly imprinted sol-gel silica, Chem. Soc. Rev. 43 (2014) 911–933.
[12] C. Alexander, H.S. Andersson, L.I. Andersson, R.J. Ansell, N. Kirsch, I.A. Nicholls, J. O'Mahony, M.J. Whitcombe, Molecular imprinting science and technology: a survey of the literature for the years up to and including 2003, J. Mol. Recognit. 19 (2006) 106–180.
[13] K. Haupt, K. Mosbach, Molecularly imprinted polymers and their use in biomimetic sensors, Chem. Rev. 100 (2000) 2495–2504.
[14] Y. Kitayama, K. Yoshikawa, T. Takeuchi, Post-cross-linked molecular imprinting with functional polymers as a universal building block for artificial polymeric receptors, Macromolecules 50 (2017) 7526–7534.
[15] Z. Zhang, X. Zhang, B. Liu, J. Liu, Molecular imprinting on inorganic nanozymes for hundred-fold enzyme specificity, J. Am. Chem. Soc. 139 (2017) 5412–5419.
[16] M. Reinmöller, M. Klinger, M. Schreiner, H. Gutte, Molecular imprinting: synthetic materials as substitutes for biological antibodies and receptors, Chem. Mater. 20 (2008) 859–868.
[17] T.S. Le, K. Takaomi, Hollow-fiber membrane absorbents embedded molecularly imprinted polymeric spheres for bisphenol A target, J. Membr. Sci. 384 (2011) 117–125.
[18] H. Zhang, L. Ye, K. Mosbach, Non-covalent molecular imprinting with emphasis on its application in separation and drug development, J. Mol. Recognit. 19 (2006) 248–259.
[19] C. Zheng, X.L. Zhang, W. Liu, B. Liu, H.H. Yang, Z.A. Lin, G.N. Chen, A selective artificial enzyme inhibitor based on nanoparticle-enzyme interactions and molecular imprinting, Adv. Mater. 25 (2013) 5922–5927.
[20] N. Li, Q. Zhang, J. Liu, J. Joo, A. Lee, Y. Gan, Y. Yin, Sol-gel coating of inorganic nanostructures with resorcinol-formaldehyde resin, Chem. Commun. 49 (2013) 5135–5137.
[21] L. Ma, W. Xu, S. Zhu, Z. Cui, X. Yang, A. Inoue, Anatase TiO_2 hierarchical nanospheres with enhanced photocatalytic activity for degrading methyl orange, Mater. Chem. Phys. 170 (2016) 186–192.
[22] J. Chu, Synthesis of core-shell magnetic molecular imprinted polymer by the surface RAFT polymerization for the fast and selective removal of endocrine disrupting chemicals from aqueous solutions, Environ. Pollut. 158 (2010) 2317–2323.
[23] X. Luo, F. Deng, L. Min, S. Luo, B. Guo, G. Zeng, C. Au, Facile one-step synthesis of inorganic-framework molecularly imprinted TiO_2/WO_3 nanocomposite and its molecular recognitive photocatalytic degradation of target contaminant, Sci. Adv. Mater. 47 (2014) 7404–7412.
[24] W. Liu, Q. Lei, Y. Yang, X. Liu, B. Xu, Synthesis and characterization of dibenzothiophene imprinted polymers on the surface of iniferter-modified carbon microspheres, Mater. Chem. Phys. 148 (2014) 605–613.
[25] H. Duan, T. Qiu, Z. Zhang, L. Guo, J. Ye, X. Li, The atmospheric pressure synthesis of TiO_2 @carbon nanocomposite microspheres and the enhanced photocatalytic performance, Mater. Lett. 153 (2015) 51–54.
[26] J. Hou, G. Dong, Y. Ye, V. Chen, Enzymatic degradation of bisphenol-A with immobilized laccase on TiO_2 sol–gel coated PVDF membrane, J. Membr. Sci. 469 (2014) 19–30.
[27] S.W. Lee, A. Izumi Ichinose, T. Kunitake, Molecular imprinting of azobenzene carboxylic acid on a TiO_2 ultrathin film by the surface sol-gel process, Langmuir 14 (1998) 2857–2863.
[28] D.N. Pei, A.Y. Zhang, X.Q. Pan, Y. Si, H.Q. Yu, Electrochemical sensing of bisphenol a on facet-tailored TiO_2 single crystals engineered by inorganic-framework molecular imprinting sites, Anal. Chem. 90 (2018) 3165–3173.
[29] N. Venkatachalam, M. Palanichamy, V. Murugesan, Sol–gel preparation and characterization of nanosize TiO_2 : its photocatalytic performance, Mater. Chem. Phys. 104 (2007) 454–459.
[30] H. Zhang, H. Xu, C. Zhao, Synthesis of morphology-controlled carbon hollow particles by carbonization of resorcinol–formaldehyde precursor microspheres and applications in lithium-ion batteries, Mater. Chem. Phys. 133 (2012) 429–436.
[31] Z. Wang, T. Qiu, L. Guo, J. Ye, L. He, X. Li, The synthesis of hydrophilic molecularly imprinted polymer microspheres and their application for selective removal of bisphenol A from water, React. Funct. Polym. 116 (2017) 69–76.
[32] Z. Wang, T. Qiu, L. Guo, J. Ye, L. He, X. Li, The synthesis of molecular recognition polymer particles via miniemulsion polymerization, React. Funct. Polym. 126 (2018) 1–8.
[33] S. Kurwadkar, A. Evans, D. Dewinne, P. White, F. Mitchell, Modeling photodegradation kinetics of three systemic neonicotinoids—dinotefuran, imidacloprid, and thiamethoxam—in aqueous and soil environment, Environ. Toxicol. Chem. 35 (2016) 1718–1726.
[34] A.A. Deshmukh, S.D. Mhlanga, N.J. Coville, Carbon spheres, Mater. Sci. Eng. R Rep. 70 (2010) 1–28.
[35] A. Nilchi, S. Janitabardarzi, S. Rasouligarmarodi, Sol-gel preparation of nanoscale TiO_2/SiO_2 composite for eliminating of con red azo dye, Mater. Sci. Appl. 02 (2011) 476–480.
[36] Y.-S. Ho, Effect of pH on lead removal from water using tree fern as the sorbent, Bioresour. Technol. 96 (2005) 1292–1296.
[37] G. McKay, H.S. Blair, J.R. Gardner, Adsorption of dyes on chitin. I. Equilibrium studies, J. Appl. Polym. Sci. 27 (1982) 3043–3057.
[38] B. Srikanth, R. Goutham, N.R. Badri, A. Ramprasath, K.P. Gopinath, A.R. Sankaranarayanan, Recent advancements in supporting materials for immobilised photocatalytic applications in waste water treatment, J. Environ. Manag. 200 (2017) 60–78.
[39] B. Sambandam, A. Surenjan, L. Philip, T. Pradeep, Rapid synthesis of C-TiO_2: tuning the shape from spherical to rice grain morphology for visible light photocatalytic application, ACS Sustain. Chem. Eng. 3 (2015) 1321–1329.
[40] G. Bayramoglu, M.Y. Arica, G. Liman, O. Celikbicak, B. Salih, Removal of bisphenol A from aqueous medium using molecularly surface imprinted microbeads, Chemosphere 150 (2016) 275–284.
[41] Z. Wang, T. Qiu, L. Guo, J. Ye, L. He, X. Li, The synthesis of hydrophilic molecularly imprinted polymer microspheres and their application for selective removal of bisphenol A from water, React. Funct. Polym. 116 (2017) 69–76.
[42] Y. Ren, W. Ma, J. Ma, Q. Wen, J. Wang, F. Zhao, Synthesis and properties of bisphenol A molecular imprinted particle for selective recognition of BPA from water, J. Colloid Interface Sci. 367 (2012) 355–361.
[43] C. Lai, M.-M. Wang, G.-M. Zeng, Y.-G. Liu, D.-L. Huang, C. Zhang, R.-Z. Wang, P. Xu, M. Cheng, C. Huang, H.-P. Wu, L. Qin, Synthesis of surface molecular imprinted TiO_2/graphene photocatalyst and its highly efficient photocatalytic degradation of target pollutant under visible light irradiation, Appl. Surf. Sci. 390 (2016) 368–376.